Journal of Food Engineering 336 (2023) 111195

Contents lists available at ScienceDirect

Journal of Food Engineering

journal homepage: www.elsevier.com/locate/jfoodeng

# Effect of environmental factors on the kinetics of evaporation of droplets containing bacteria or viruses on different surfaces

Alexander J. Cunliffe [a], Ru Wang [b], James Redfern [a,*], Joanna Verran [c], D. Ian Wilson [b]

[a] Department of Natural Science, Faculty of Science and Engineering, Manchester Metropolitan University, Manchester, M1 5GD, UK
[b] Department of Chemical Engineering and Biotechnology, University of Cambridge, Philippa Fawcett Drive, Cambridge, CB3 0AS, UK
[c] Department of Life Science, Faculty of Science and Engineering, Manchester Metropolitan University, Manchester, M1 5GD, UK

ARTICLE INFO

*Keywords:*
Bacterial contamination
Viral contamination
Moisture evaporation
Antimicrobial efficacy
Bacterial evaporation

ABSTRACT

The efficacy of antimicrobial surfaces at solid-air interfaces can be assessed using standardised testing methods, typically by placing a droplet inoculated with microorganisms onto the surface and monitoring changes in microbial counts over time (hours). However, the mode of action of the putative antimicrobial may rely on the presence of moisture on the surface, thus it is important to know the time taken for the inoculum to dry, since this will affect resultant counts and thereby deduction as to the efficacy of the antimicrobial.

Droplet (+/− microorganisms) evaporation time was measured on four different surfaces (copper, PVC, polypropylene and nitrile rubber) where temperature, relative humidity and airflow in the test chamber were controlled. The data were compared with simple models based on external mass transfer for predicting the evaporation time: (i) one assuming constant wetted area (CWA), where the diameter of the drop is unchanged but the volume/height decreases; (ii) constant contact angle (CCA), where the diameter of the droplet decreases but the droplet profile/contact angle remains unchanged; and (iii) a mixed mode model.

The mixed mode model gave the best fit to the data, in which evaporation initially followed CWA kinetics, then shifted to CCA when a critical contact angle was reached. The presence of microorganisms consistently and often significantly reduced the evaporation time. Deposited bacteria were visible over the whole wetted area, with a noticeable ring at the original edge of the droplet (the location of the initial solid-liquid-air contact line), consistent with the mixed mode model.

Accumulation of microorganisms and the decrease in evaporation time may affect the effectiveness of antimicrobial materials. The speed of droplet evaporation is affected by a wide range of factors: temperature, humidity, airflow, the nature of the surface and the presence (and nature) of microorganisms. If these factors are not adequately recognised or controlled, then results from testing methods carried out under different (unspecified) environmental conditions in different laboratories, are liable to vary and give rise to confusion and misinterpretation.

## 1. Introduction

There is widespread interest in the development of active, non-porous surfaces as part of a microbial control strategy. Much of the work in this area has focused on combatting bacterial (and spore) infection but recent events have seen a concerted effort on developing surfaces which are effective at deactivating viruses (Kumari and Chatterjee, 2021). Due to the increasing threat of antimicrobial resistance and increasing awareness and ongoing impact of viral pandemics and understanding that pathogens such as SARS-CoV-2 can remain viable on surfaces for extended periods of time (Chatterjee et al., 2021), novel approaches to controlling microorganisms in indoor settings is likely to remain a priority. As such, many novel methods for generating antimicrobial surfaces are being reported in the literature, e.g. metallic metals such as copper and topographical changes, coatings, and inclusion of nano- and/or photocatalytic materials, (Grass et al., 2011; Hansan et al., 2020; Imani et al., 2020; Ratova et al., 2018). Testing of such surfaces is often based on standardised methods (Cunliffe et al., 2021), designed to enhance lab-to-lab reproducibility (although this is not always achieved). However, the conditions that the methods stipulate are not always applicable to the conditions likely found in the intended end-use environment, such as hospitals. An example of this is relative humidity

* Corresponding author.
*E-mail address:* J.Redfern@mmu.ac.uk (J. Redfern).

https://doi.org/10.1016/j.jfoodeng.2022.111195
Received 25 February 2022; Received in revised form 19 June 2022; Accepted 21 June 2022
Available online 27 June 2022

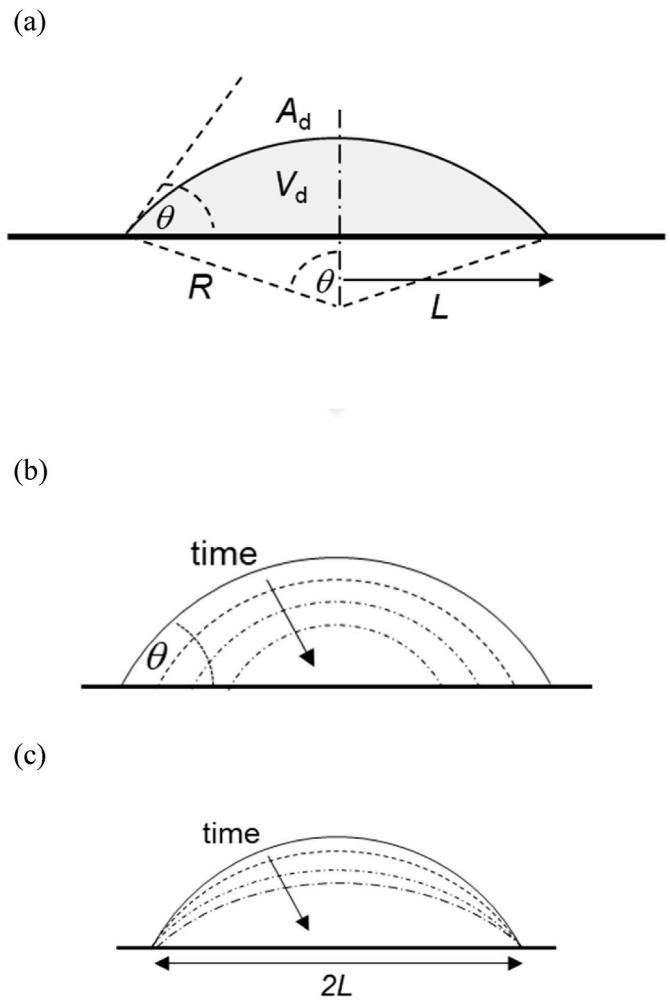


**Fig. 1.** Schematics of small sessile drops undergoing evaporation. The Bond number is small so surface tension dominates gravity and the drop shape is a truncated sphere. (*a*) Geometry, showing drop volume $V_d$, liquid-air interface area $A_d$, drop radius $R$, wetted radius $L$ and contact angle $\theta$. Droplet evaporating under (*b*) constant contact angle (CCA) mode, $L$ decreases over time, and (*c*) constant wetted area mode (CWA: $L$ constant, $\theta$ decreases over time).

(RH), which determines whether a water film will be present on a surface and how long it would take to dry. A second is the presence of convective air currents generated by ventilation, draughts and motion of personnel, which enhance the transport of heat and mass involved in evaporation. In many standardised antimicrobial test methods, such as the commonly used BS ISO 22196 (BS ISO 22196, 2011), relative humidity is kept artificially high (>90%) and airflow is absent. Since the efficacy of many antimicrobial coatings and surfaces may rely on the presence of moisture, *e.g.* metallic silver (Rai et al., 2009), the ability to predict moisture evaporation times is needed in order to be able to relate laboratory tests to application. This study focuses on humidity and temperature: the effect of convection is demonstrated in benchmarking studies with water and is not considered further here.

Redfern et al. (2018) developed a surface testing chamber which allowed the temperature and relative humidity of the atmosphere, as well as local air flow velocity, to be controlled independently of one another. They showed that the size of water droplets as well as these environmental parameters determined the time taken for a drop of water to evaporate. They fitted their data to a generalised quadratic model which fitted the data reasonably well ($R^2 = 0.872$) and demonstrated the importance of the four factors. One of the challenges with such empirical models is that they are not suited for extrapolation, that is, to predict the result when another parameter is altered: further testing (for training the model) is required.

In this paper we demonstrate that Redfern et al.'s results are consistent with the predictions of a first order quantitative model based on external mass transfer control. Several workers have presented models for droplet evaporation under well-controlled quasi-stagnant air conditions (*e.g.* Hu and Larson, 2002), and used these to demonstrate the effect of tailored surfaces (*e.g.* Sobac et al., 2011) on evaporation. The interest in the 'coffee ring effect' observed when droplets of colloidal suspensions evaporate (*e.g.* Deegan et al., 1997, 2000) has prompted extensive work in this area, including phenomena such as Marangoni flows arising from variation in surface tension generated by non-uniform temperature and concentration profiles. These effects are not considered here.

The nature of the surface influences the rate of evaporation through the behaviour of the three-phase contact line (where the air, solid and liquid interfaces coexist): on a homogeneous solid with no preferential concentration of suspended or dissolved species at the contact line, one would expect the droplet to exhibit a constant contact angle (CCA), $\theta$ (Fig. 1(a)) and retain its shape (but not diameter) as it dried, labelled CCA behaviour (Fig. 1(b). With heterogeneous surfaces, effects such as contact line pinning can give rise to a constant wetted solid surface area ($\pi L^2 = \pi(R\sin\theta)^2$, Fig. 1(c)), altering the surface area to volume ratio for the droplet. This is labelled constant wetted area (CWA) behaviour. Other factors determine the transition between CCA and CWA behaviour: for instance, Soulié et al. (2015) observed CCA behaviour in water and saline solutions with NaCl concentrations $<10^{-6}$ M, and CWA behaviour at higher concentrations. This study employs droplets with saline or buffer concentrations above this threshold.

We show that the variation in Redfern et al.'s data for evaporation of water drops can be related to mixed contact line behaviour, involving CWA behaviour initially while the shape of the drop changes from advancing contact angle, $\theta_a$, to receding contact angle, $\theta_r$, mode (appropriate for a shrinking droplet) followed by shrinkage subject to CCA behaviour (*i.e.* pinned but then shrinks). This demonstrates that the mode of evaporation cannot be assumed to be simply CWA or CCA, and should be taken into account by those interested in the rate at which evaporation occurs from an antimicrobial material, due to the length of time evaporation takes to occur being likely to determine the length of time an antimicrobial material remains active.

The phenomenology underpinning advancing and retreating contact angles is described by Bormashenko (2017): note that $\theta_a - \theta_r > 0$ even for uniform homogeneous surfaces. Contact line pinning is known to arise with the evaporation of suspensions (*e,g.* Deegan et al., 2000). The evaporation of concentrated colloidal suspensions and polymer solutions has been studied at length (*e.g.* Larson, 2014; Soulié et al., 2015; Eales et al., 2016) owing to interest in inkjet applications and to the 'coffee ring effect' where a layer or layers of particles is deposited at the initial contact line. Aerosols contaminated by bacteria and other microorganisms represent examples of dilute suspensions, and thus the effect of the presence of microorganisms in the droplets on the rate of droplet evaporation and the pattern of deposition on non-porous surfaces are also investigated in this study. Deleplace et al. (2022) recently presented studies of 'coffee rings' and other deposition patterns generated by evaporation of droplets containing hydrophobic and hydrophilic *Bacillus* spores on stainless steels, polypropylene and glass. They outlined the importance of these factors to process and product hygiene, and the consequences of the deposit patterns on the ease of removal of the organisms using a rinsing or cleaning procedure. They observed noticeable differences arising from surface and organism properties. Deposits that had not dried completely were significantly more resistant to cleaning. Their analysis did not, however, link the observations to evaporation rates.

Few workers have considered the effect of forced convection on droplet evaporation. Investigations of mass transfer from droplets in duct flows (*e.g.* Coutant and Penski, 1982) tend to feature well-defined

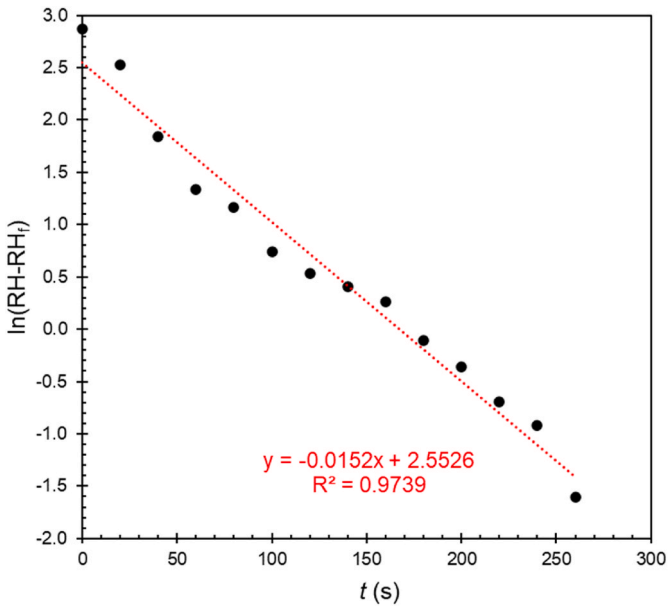


**Fig. 2.** Approach of chamber relative humidity, RH, to equilibrium value, $RH_f$, following closure of the chamber lid. The initial value (relative humidity in the room) was 23% and $RH_f$ (saturated $K_2CO_3$ solution) 43%. Data are plotted in the form of Equation [A3].

duct geometries, where the enhancement of drying by convection can be discussed in terms of a Reynolds number for the bulk flow based on the hydraulic diameter as well as a Reynolds number based on the initial droplet dimensions. Well defined flow conditions are rarely observed in practice and we briefly establish the significance of the convective contribution in Redfern et al.'s tests for aqueous solutions: the impact of an external shear force on the droplet shape and Marangoni effects is beyond the scope of the simple mass transfer models presented here and a study of convective effects on evaporation of droplets containing organisms represents a subject for further work.

The findings of this work can be strengthened by more in-depth and detailed experimentation and analysis, including direct monitoring of the shape of the droplets to confirm the behaviour postulated here. The current study employs a first order model describing evaporation, and there is considerable scope for including the contributions included in more detailed modelling approaches.

## 2. Modelling

### 2.1. Transient chamber conditions

A detailed description of the chamber is given by Redfern et al. (2018) and a summary is provided in the Supplementary Information. The temperature was controlled by a heating pad and the relative humidity inside the chamber was set by Petri dishes containing saturated salt solutions. The chamber's use of side compartments to introduce test surfaces on which droplets had been deposited minimised the impact of this operation on the humidity (and relative humidity, RH) within the chamber. Fig. 2 shows that it took around 4 min to re-establish equilibrium in the chamber when the lid had been opened, which would

**Table 1**
Summary of water droplet evaporation tests by Redfern et al. (2018) on polypropylene.

| Volume (μL) | $R_0$ (mm) | *Bo* (−) | Temperature (°C) | Relative humidity (%) | $t_c$ (s) |
|---|---|---|---|---|---|
| 2 | 1.05 | 0.15 | 21.5–31.2 | 27.3–63.7 | 32–99 |
| 5 | 1.42 | 0.27 | 22.6–29.2 | 35.4–68.6 | 69–169 |
| 10 | 1.79 | 0.43 | 21.5–31.3 | 25.8–62.7 | 92–287 |
| 20 | 2.26 | 0.69 | 21.7–31.2 | 25.5–61.8 | 146–455 |

**Table 2**
Advancing contact angles (± standard deviation) measured for 1 μL droplets. All values are rounded to the nearest whole number. Asterisk denotes where contact angle is significantly different ($p < 0.05$) between 1 μL (below) and 5 μL (Table 3) measurements.

| Liquid | Organism | Polypropylene | Nitrile | PVC | Copper |
|---|---|---|---|---|---|
| Water | – | 82° (±3°) | 97° (±4°) | 60° (±2°) | 74° (±3°) |
| Saline | – | 84° (±1°)* | 104° (±2°) | 65° (±7°) | 68° (±4°) |
| Saline | *E. coli* | 86° (±4°) | 93° (±2°) | 64° (±6°) | 51° (±6°) |
| Saline | *P. syringae* | 79° (±2°) | 95° (±4°) | 71° (±6°) | 65° (±9°) |
| SM buffer | – | 85° (±4°) | 100° (±6°) | 59° (±8°) | 58° (±6°) |
| SM buffer | *Phi6* | 82° (±2°) | 88° (±5°) | 64° (±3°) * | 63° (±3°) |
| SM buffer | *PhiX174* | 83° (±2°) | 78° (±2°) | 65° (±3°) | 71° (±2°) |

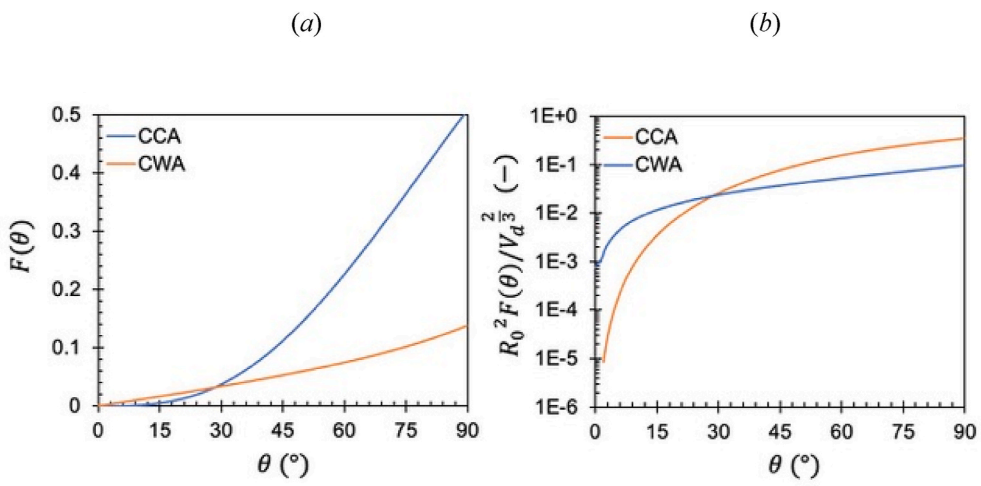


**Fig. 3.** Effect of contact angle on geometric functions (*a*) $F_\theta$ (CCA mode) and $F_L$ (CWA mode), Equations [5] and [8], respectively. (*b*) Scaled products, $R_0^2 F_\theta / V_d^{2/3}$ and $R_0^2 F_L / V_d^{2/3}$, for initial droplet volume $V_d = 2\ \mu$L. For CWA, $\theta$ is the initial contact angle as $\theta \to 0$ as the drop evaporates. Note the log scale on the ordinate axis in (*b*).

**Table 3**
Advancing contact angles (± standard deviation) measured for 5 μL droplets. All values are rounded to the nearest whole number. Asterisk denotes where contact angle is significantly different ($p < 0.05$) between 1 μL (Table 2) and 5 μL (below) measurements.

| Liquid | Organism | Polypropylene | Nitrile | PVC | Copper |
|---|---|---|---|---|---|
| Water | – | 79° (±0°) | 101° (±7°) | 57° (±9°) | 68° (±4°) |
| Saline | – | 81° (±1°)* | 104° (±2°) | 70° (±9°) | 64° (±2°) |
| Saline | *E. coli* | 80° (±1°) | 96° (±2°) | 62° (±2°) | 49° (±3°) |
| Saline | *P. syringae* | 78° (±1°) | 95° (±2°) | 67° (±5°) | 66° (±5°) |
| SM buffer | – | 82° (±1°) | 100° (±6°) | 73° (±4°) | 54° (±6°) |
| SM buffer | *Phi6* | 88° (±5°) | 96° (±3°) | 75° (±1°)* | 59° (±6°) |
| SM buffer | *PhiX174* | 84° (±1°) | 90° (±5°) | 60° (±6°) | 68° (±2°) |

introduce undesirable transients into any droplet evaporation study, where the evaporation times ranged from 30 to 450 s. The data are plotted in the form $ln(\text{RH-RH}_{\text{final}})$ vs. time $t$ as this is the trend predicted by mass transfer control models (see Appendix). When the side compartments were used the RH did not change by more than a few percent.

### 2.2. Drop evaporation

This work considers droplets with Bond numbers <1,[1] so the droplet shape can be approximated as a spherical cap (a truncated sphere, see Fig. 1) and the surface area and volume estimated using geometric relationships. The droplet is assumed to be at constant temperature, *i.e.* heat transfer limitations do not arise nor Marangoni effects arising from temperature differences over the drop. The rate of droplet evaporation will be proportional to the area of the liquid/air interface, $A_d = 2\pi R^2(1 - \cos\theta)$, while its volume is given by $V_d = \frac{1}{3}\pi R^3(2 + \cos\theta)(1 - \cos\theta)^2$. For a drop of liquid with molar density $\rho_m$, the rate of mass transfer in the absence of thermal effects can be written as

$$\frac{d}{dt}(V_d\rho_m) = -A_d\bar{k}_m C_T(y^* - y_b) \quad [1]$$

where $y_b$ is the mol fraction of the evaporating species in the chamber vapour space (related to the humidity, $H$), $y^*$ is that in equilibrium with the drop, $C_T$ the molar concentration in the vapour phase and $\bar{k}_m$ is an average mass transfer coefficient. Redfern et al. studied water droplets so changes in concentration and vapour pressure over time did not arise. Experiments conducted in the current work also considered aqueous salt and buffer solutions, where the concentration is expected to change over time: the impact of the presence of salts is discussed.

In estimating an evaporation time, we assume quasi-steady state, which is expected to apply as the contact angles considered are not small. Writing $\bar{k}_m$ in terms of the dimensionless mass transfer coefficient for a sphere, the Sherwood number, $\overline{Sh} \equiv 2R\bar{k}_m/D$ (where $D$ is the diffusivity of evaporating species in air), gives

$$\frac{d}{dt}(V_d) = -\frac{A_d}{2R}\frac{DC_T\overline{Sh}}{\rho_m}(y^* - y_b) \quad [2]$$

We consider three scenarios: (*i*) constant contact angle, where the droplet radius $R$ decreases from its initial value, $R_0$, to zero (Fig. 1(b)); (*ii*) constant wetted area, where dimension $L = R_0\sin\theta_0$ is constant due to contact line pinning or other effects and $\theta$ decreases over time (Fig. 1 (c)); and (*iii*) mixed mode, where CWA behaviour is observed initially as the droplet, with shape initially set by the advancing contact angle $\theta_a$, changes to that given by the receding contact angle as liquid evaporates,

[1] The Bond number $Bo = g\Delta\rho R^2/\gamma$ compares gravitational forces to capillary ones. Here $\gamma$ is the liquid-air surface tension, $g$ is the gravitational constant, $R$ is the droplet radius and $\Delta\rho$ is the difference in density between the liquid and air.

**Table 4**
Effect of droplet composition on evaporation times, with reference to CCA model (Figs. 6–9). Anova and Tukey HSD tests determined pairwise statistical significance ($p < 0.05$), with ~ denoting no significant difference but observed increase in evaporation time, and > denoting a statistically significant difference supporting the observed increase in evaporation time. SMB – SM buffer.

| Surface | Humidity range | Droplet volume | Trend in evaporation times | |
|---|---|---|---|---|
| | | | Liquids | Suspensions |
| Polypropene | Low | 1 μL | SMB ~ saline > water | Saline > *E. coli* ~ *P. syringae* SMB ~ *Phi X174* ~ *Phi6* |
| | | 5 μL | SMB ~ saline > water | Saline ~ *E. coli* ~ *P. syringae* SMB ~ *Phi X174* ~ *Phi6* |
| | Mid | 1 μL | SMB > Saline > water | Saline > *P. syringae* ~ *E. coli* SMB > *Phi6* ~ *Phi X174* |
| | | 5 μL | SMB ~ Saline ~ water | Saline ~ *E. coli* ~ *P. syringae* SMB > *Phi6* > *PhiX174* |
| Nitrile | Low | 1 μL | Water ~ saline ~ SMB | Saline > *E. coli* > *P. syringae* SMB > *Phi X174* > *Phi6* |
| | | 5 μL | Water ~ Saline ~ SMB | Saline ~ *P. syringae* ~ *E. coli* SMB ~ *Phi X174* ~ *Phi6* |
| | Mid | 1 μL | SMB ~ saline ~ water | Saline ~ *P. syringae* ~ *E. coli* SMB ~ *Phi6* ~ *Phi X174* |
| | | 5 μL | SMB ~ water ~ saline | Saline > *E. coli* > *P. syringae* SMB > *Phi6* > *Phi X174* |
| Copper | Low | 1 μL | SMB ~ Saline ~ water | Saline > *E. coli* ~ *P. syringae* SMB > *Phi X174* > *Phi6* |
| | | 5 μL | Saline ~ SMB ~ water | Saline ~ *P. syringae* > *E. coli* SMB ~ *Phi X174* ~ *Phi6* |
| | Mid | 1 μL | Saline ~ SMB > water | Saline ~ *E. coli* > *P. syringae* SMB > *Phi6* ~ *Phi X174* |
| | | 5 μL | Water ~ Saline ~ SMB | Saline > *P. syringae* ~ *E. coli* SMB > *Phi X174* > *Phi6* |
| PVC | Low | 1 μL | Saline ~ SMB ~ water | Saline ~ *E. coli* > *P. syringae* SMB > *Phi6* ~ *Phi X174* |
| | | 5 μL | SMB ~ saline > water | Saline ~ *P. syringae* > *E. coli* SMB ~ *Phi X174* ~ *Phi6* |
| | Mid | 1 μL | Saline ~ SMB > water | Saline ~ *P. syringae* > *E. coli* SMB > *Phi X174* > *Phi6* |
| | | 5 μL | SMB ~ saline ~ water | Saline > *P. syringae* ~ *E. coli* SMB ~ *Phi X174* ~ *Phi6* |

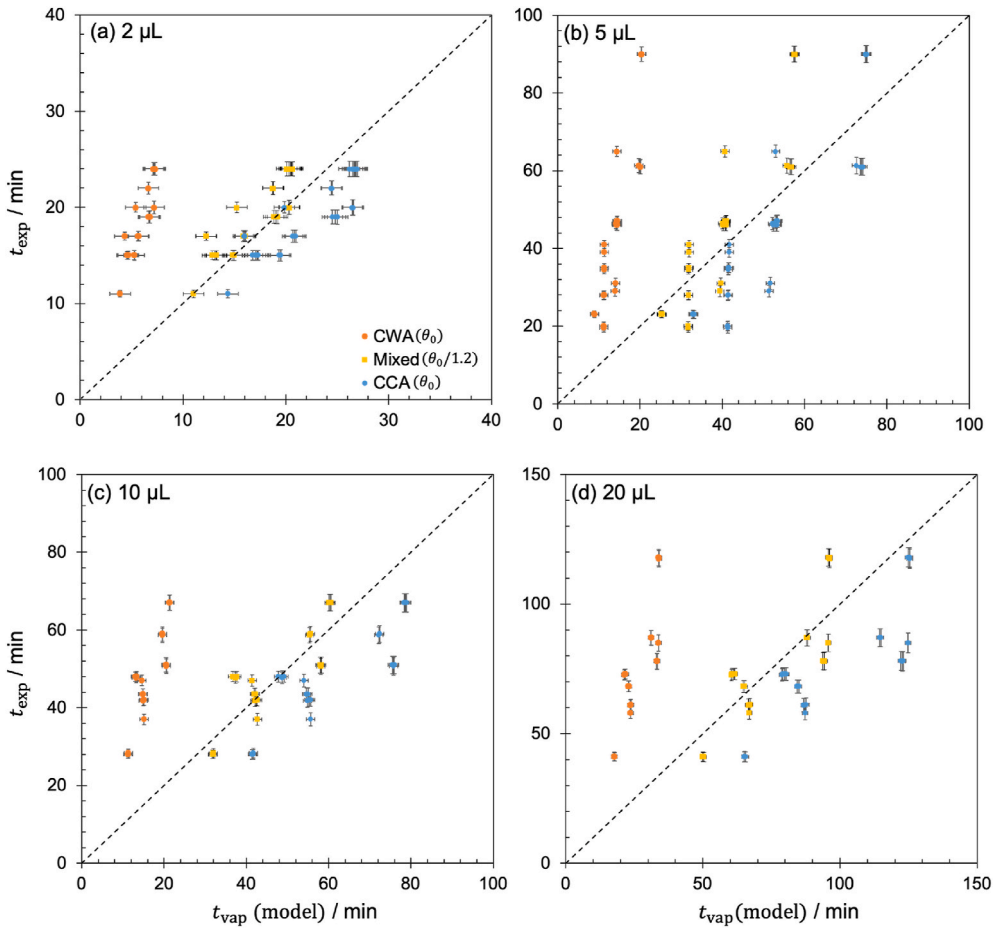


**Fig. 4.** Comparison of evaporation times of water droplets (Redfern et al., 2018) in stagnant air with model prediction for CCA mode (blue symbols), CWA (orange symbols), and mixed, for $\theta_r = \theta_0/1.2$ (yellow symbols) for drops with initial volume of (a) 2 μL, (b) 5 μL, (c) 10 μL and (d) 20 μL. Dashed locus shows the line of equality, *i.e.* $y = x$. Vertical error bars indicate the range in experimental values: horizontal error bars indicate the uncertainty in the model predictions.

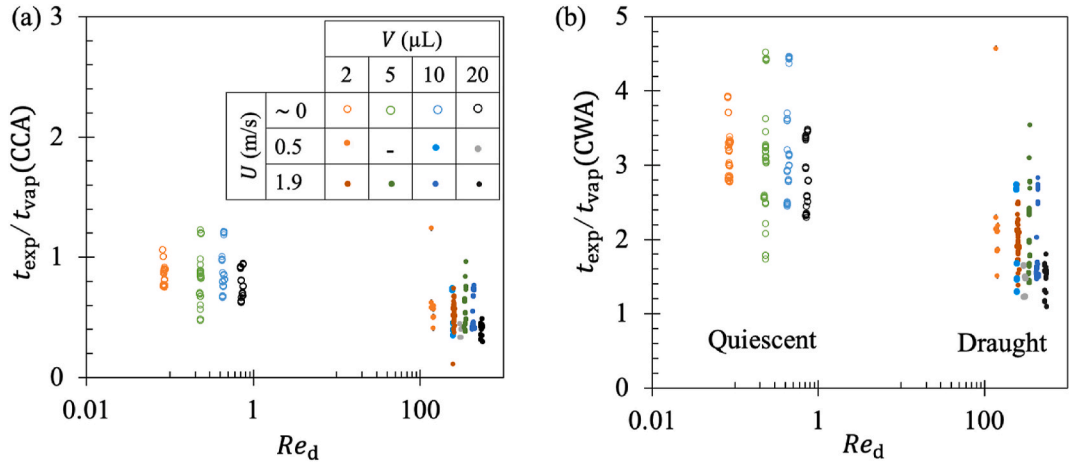


**Fig. 5.** Effect of convection, expressed as droplet Reynolds number, on evaporation time for water droplets. For the purposes of illustration, a mean velocity of 1 mm $s^{-1}$ is used in the calculation of the Reynolds number for the quasi-static cases ($Re_d \sim 0$ for these cases). The evaporation time is scaled by the predicted evaporation time in stagnant air for (*a*) CCA mode, and (*b*) CWA mode. Symbols: hollow, quiescent; solid, fan on.

followed by CCA behaviour with $\theta = \theta_r$.

(i) Constant contact angle, CCA

Writing $\Delta y = (y^* - y_b)$ and introducing the above expressions for $V_d$ and $A_d$ for fixed $\theta$ gives:

$$R\frac{dR}{dt} = \frac{1}{2}\frac{dR^2}{dt} = -\frac{1}{(2+\cos\theta)(1-\cos\theta)}\frac{DC_T\Delta y}{\rho_m}\overline{Sh} \quad [3]$$

Integrating from initial radius $R_0$ at time zero gives

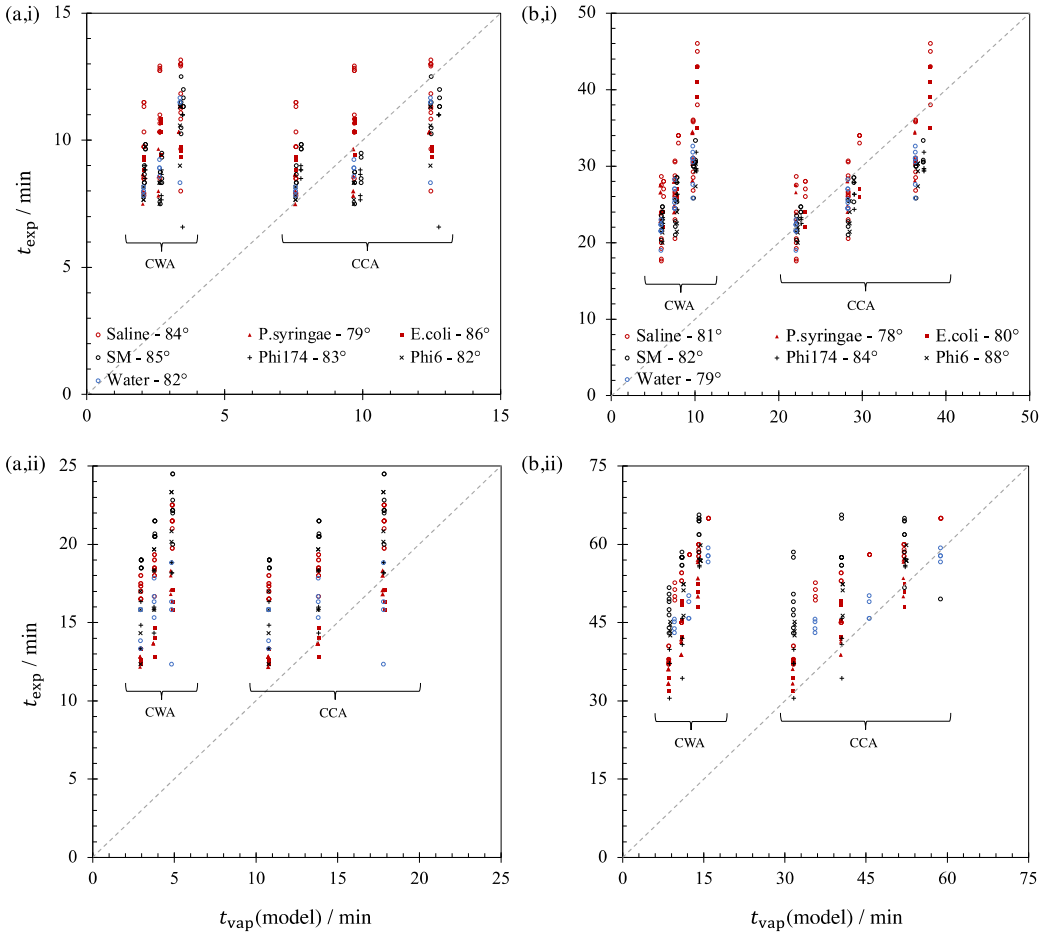


**Fig. 6.** Comparison of liquid drop evaporation times in stagnant air on polypropylene with CCA and CWA model predictions. Liquid drops with initial volume of (i) 1 μL or (ii) 5 μL, and at (*a*) low humidity and (*b*) mid humidity. The three groups in each plot correspond to temperatures of 22, 26 and 30 °C (with higher temperature giving shorter evaporation time). Dashed locus shows the line of equality, *i.e.* $y = x$. *P. syringae* and *E. coli* prepared in saline, *Phi X174* and *Phi6* in SM buffer. The contact angle indicated in the legend is the measured static contact angle of the liquid drop on the polypropylene surface (see Tables 2 and 3).

$$R_0^2 - R^2 = -\frac{2}{(2+\cos\theta)(1-\cos\theta)}\overline{Sh}\frac{DC_T\Delta y}{\rho_m}t \quad [4]$$

and a time for droplet evaporation, $t_{vap}$, of

$$t_{vap} = \left[\frac{(2+\cos\theta)(1-\cos\theta)}{2\overline{Sh}}\right]\left[\frac{\rho_m R_0^2}{DC_T\Delta y}\right] = F_\theta t_c \quad [5]$$

where $F_\theta$ is a geometric function and $t_c$ is a characteristic timescale for droplet evaporation. For the case of a hemispherical drop ($\theta = \pi/2$, symmetrical), $\overline{Sh} = 2$ and $F_\theta = 1/2$. For other values of $\theta$ the local flux varies over the interface: Hu and Larson (2002) reported the following result for $0 \le \theta \le \pi/2$ for evaporation controlled by external mass transfer:

$$\frac{d}{dt}(\rho_m V_d) = -\pi R D C_T \Delta y\left(0.27\theta^2 + 1.30\right) \quad [6]$$

which, when substituted into [2], gives the dependency of $F_\theta$ on $\theta$ shown in Fig. 3. Contributions from natural convection are neglected. Smaller contact angles increase the interfacial area per unit droplet volume and, for the constant $\theta$ case, shorten the evaporation time for a given value of $R_0$.

For a given droplet volume, as used in these experiments, $R_0$ depends on $\theta$. Equation [5] indicates that the value of $\theta$ affects the drying time for a droplet of initial volume $V_d$ via the product $R_0^2 F_i$, where $R_0 \propto \{V_d/(2+\cos\theta)(1-\cos\theta)^2\}^{1/3}$ and subscript $i$ denotes the drying mode.

The other parameters in the characteristic drying time do not depend on the drop size in this model. Fig. 3(*b*) shows how the product $R_0^2 F_\theta / V_d^{2/3}$ varies with $\theta$ for $1 \le \theta \le 90°$ (the product is scaled by the characteristic area associated with the droplet volume, $V_d^{2/3}$, to make it dimensionless). The plot shows that $R_0^2 F_\theta$ (and thus the drying time) is very sensitive to $\theta$ for $\theta \le 45°$: over the range of $\theta$ values of interest in this work (Tables 2 and 3, 45–90°) the CCA result increases modestly with $\theta$.

The above result indicates that selecting a surface so that a liquid will spread on it (small $\theta$) therefore has the counter-productive property for antimicrobial materials which rely on the surface being wet, as this can enhance the rate at which the liquid evaporates, limiting the amount of time the surface will remain antimicrobial. It should be noted that the CCA model is not valid for $\theta \sim 0$ (when the drop is effectively a puddle).

(ii) Constant wetted area, CWA

When the contact line is pinned, the radius of the wetted area, $L$, remains constant, and the contact angle changes over time as the volume of the drop decreases. Using the Hu and Larson result, Equation [2] becomes:

$$\frac{1}{3}\frac{(1-\cos\theta)^2}{\sin^4\theta\left(0.27\theta^2+1.30\right)}d\theta = -\frac{DC_T\Delta y}{\rho_m R_0^2 \sin^2\theta_0}dt \quad [7]$$

Integrating from $\theta_0$ to zero gives

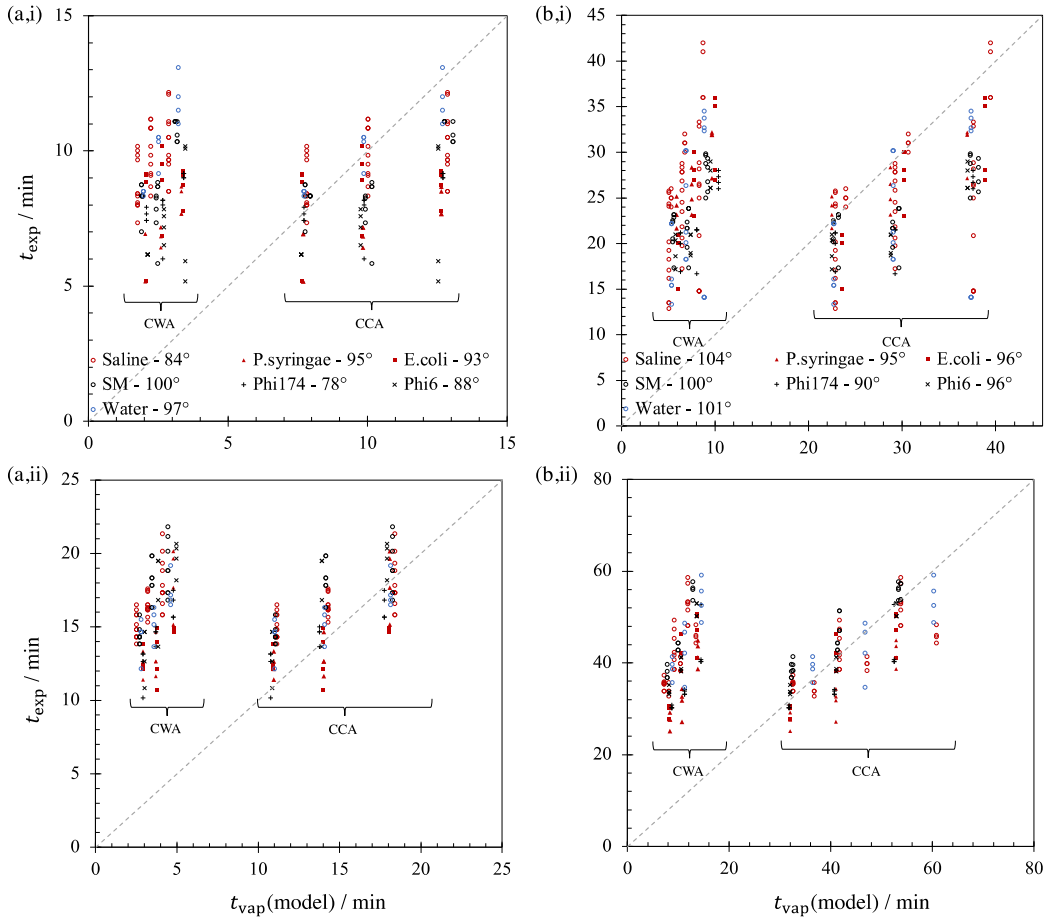


**Fig. 7.** Comparison of liquid drop evaporation times in stagnant air on nitrile with CCA and CWA model predictions. Liquid drops with initial volume of (i) 1 μL or (ii) 5 μL, and at (*a*) low humidity and (*b*) mid humidity at temperatures of 22, 26 and 30 °C. Dashed locus shows the line of equality, *i.e.* $y = x$. *P. syringae* and *E. coli* prepared in saline, *Phi X174* and *Phi6* in SM buffer. The contact angle indicated in the legend is the measured static contact angle of the liquid drop on the nitrile surface (see Tables 2 and 3).

$$t_{vap} = \left\{ \frac{\sin^2\theta_0}{3} \int_0^{\theta_0} \frac{(1-\cos\theta)^2}{\sin^4\theta\left(0.27\theta^2 + 1.30\right)} d\theta \right\} \left[ \frac{\rho_m R_0^2}{DC_T \Delta y} \right] = F_L t_c \qquad [8]$$

with the *same* characteristic timescale. Fig. 3 shows that a smaller contact angle again results in a shorter evaporation time. Comparing $F_\theta$ and $F_L$, there is a transition at 28° indicating that for strongly wetting liquids (small $\theta$) a droplet following CCA behaviour for a given $\theta$ will evaporate completely in a shorter time.

Fig. 3(b) shows the effect of initial contact angle on evaporation of droplets of equal initial volume. The drying time increases with $\theta$, as in the CCA case, but the range is noticeably smaller, varying by 1½ decades compared to 4½ decades for CCA. The two values are similar for $\theta \sim 28°$, with CWA times significantly larger for the CWA mode on surfaces that encourage wetting (low $\theta$).

(iii) Mixed model

In the mixed model, the droplet evaporates initially with constant wetted area as the contact angle decreases from $\theta_0 = \theta_a$ until it reaches $\theta_r$. Thereafter, the decrease in volume of the drop is modelled as the wetted area decreasing following CCA behaviour, with $\theta = \theta_r$. Combining the CWA and CCA models, the evaporation time is given by:

$$\frac{t_{vap}}{t_c} = \left\{ \frac{\sin^2\theta_0}{3} \int_{\theta_r}^{\theta_0} \frac{(1-\cos\theta)^2}{\sin^4\theta\left(0.27\theta^2 + 1.30\right)} d\theta + \left[ \frac{(2+\cos\theta)(1-\cos\theta)}{2\overline{Sh}} \right] \right\} \qquad [9]$$

For a given liquid, $t_c$ is set by the size of the droplet and the atmospheric conditions. The contact angles and the kinetic factors, *e.g.* $F_L$ and $F_\theta$, are determined by the surface and its interaction with the droplet. Comparison of the evaporation times with the model predictions will indicate how long the surface remains wetted and thus the likelihood of antimicrobial activity.

## 3. Materials and methods

### 3.1. Preparation of materials and chamber

Non-porous test sections measuring 10 mm × 10 mm were cut from copper (CuSn5), polyvinyl chloride (PVC), polypropylene and nitrile sheet. Prior to use, all sections were wiped thoroughly with cloth soaked in 70% ethanol and left to dry in aseptic conditions for 60 min. Sections were secured to a polystyrene base plate (127.7 × 85.4 mm) using double-sided tape and placed inside the environmental control chamber. The environmental control chamber (internal dimensions 296 mm × 171 mm × 51 mm) allowed temperature and relative humidity (RH) to be controlled independently. To maintain the desired RH, saturated solutions of lithium chloride (180 g and 60 mL of water, producing a RH of 15%) or potassium carbonate (200 g and 60 mL of water, producing a

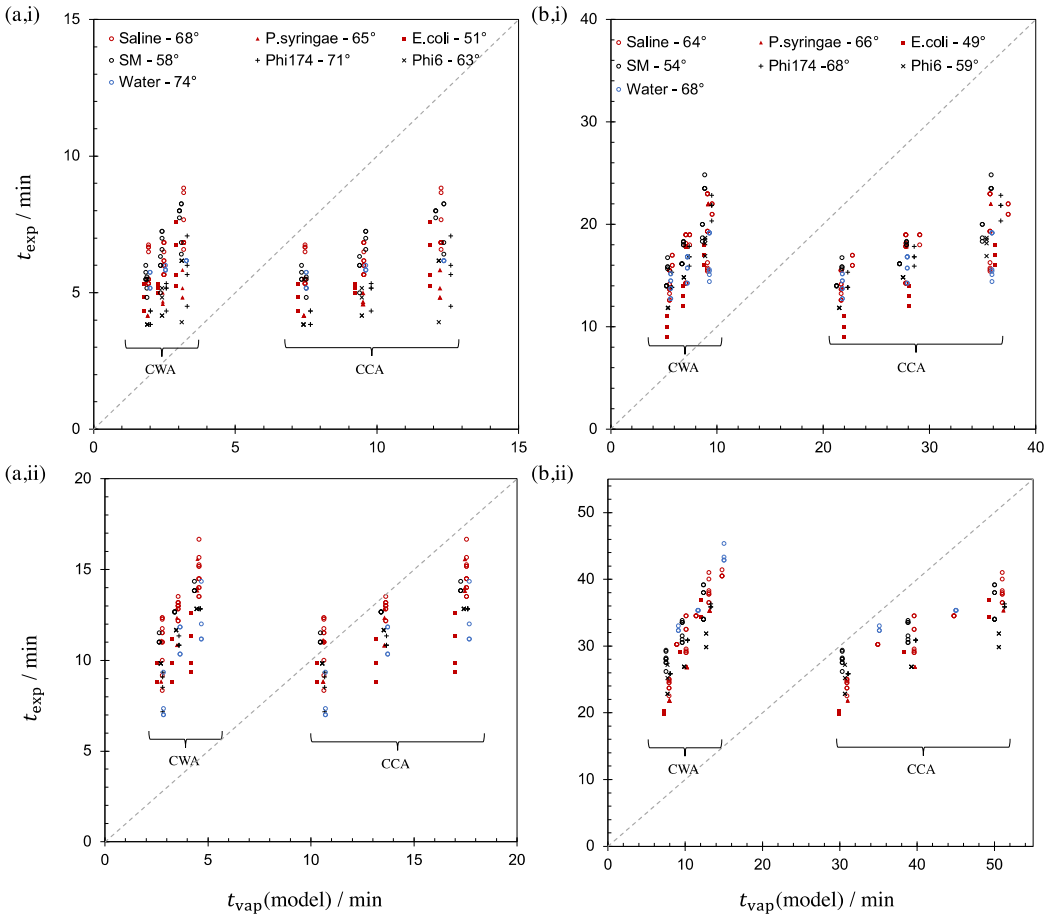


**Fig. 8.** Comparison of liquid drop evaporation times in stagnant air on copper with CCA and CWA model predictions. Liquid drops with initial volume of (i) 1 μL or (ii) 5 μL, and at (*a*) low humidity and (*b*) mid humidity at temperatures of 22, 26 and 30 °C. Dashed locus shows the line of equality, *i.e.* $y = x$. *P. syringae* and *E. coli* prepared in saline, *Phi X174* and *Phi6* in SM buffer. The contact angle indicated in the legend is the measured static contact angle of the liquid drop on the copper surface (see Tables 2 and 3).

RH of 40%) were distributed evenly across four Petri dishes inside the chamber and RH monitored using a HD500 sensor and datalogger (Extech Instruments). Temperature was adjusted and maintained with a propagation heat mat (PVC, 18 W, 220 V) and monitored with a thermostat (Vivosun, Shanghai, China).

### 3.2. Preparation of solutions and microbial suspensions

Deionised water was sterilised by autoclaving at 121 °C for 15 min. Saline solutions were prepared as 0.85 wt% NaCl (ThermoFisher Scientific) in deionised water and sterilised by autoclaving. SM buffer was prepared by adding 5.8 g of NaCl, 2 g of $MgSO_4{\cdot}6H_2O$ and 50 mL 1 M Tris-Cl pH 7.5–800 mL distilled water and mixed until dissolved, adjusted to 1 L with distilled water and sterilised by autoclaving at 121 °C for 15 min. Tris-Cl was prepared by adding 12.11 g of 1 M tris base to 80 mL distilled water and mixed until dissolved with the pH adjusted to 7.5 by adding 30 wt% HCl. Both the saline and buffer solution concentrations are large compared to the concentration at which Soulié et al. (2015) reported the onset of CWA behaviour.

Bacteria were maintained as streak (purity) plates on tryptone soya agar (TSA) at 4 °C until required. *Escherichia coli* (ATCC 13706) and *Pseudomonas syringae* (ATCC 21781) cultures were prepared for the experiments by inoculating one colony of bacteria from the respective streak plates, transferring to 10 mL TSB and incubating at 37 °C and 28 °C, respectively, for 24 h. Bacterial cultures were then centrifuged at 3500 rpm for 10 min. The supernatant was removed, and 10 mL sterile saline added, with the resultant suspension mixed by vortex (this process was repeated once). Suspensions were then adjusted to 0.5OD at 600 nm (determined by spectrophotometer (Jenway)) using sterile saline.

Bacteriophage Phi6 (ATCC 21781-B1) and PhiX174 (ATCC 13706-B1) suspensions were prepared following a standard phage assay protocol (Adams, 1959). In brief, a 10-fold serial dilution of stock phage was performed up to $10^{-8}$ in SM buffer. Subsequently, for each dilution, 100 μL of bacteriophage was mixed with 100 μL of corresponding bacterial overnight culture (*Pseudomonas syringae* (ATCC 21781) for Phi6 and *Escherichia coli* (ATCC 13706) for Phi ×174) and 3 mL of soft (0.7% w/v) molten (45–55 °C) TSA and poured onto a regular strength TSA agar plate. Following an 18-h incubation (30 °C), any plaques present on each dilution were counted and used to calculate the number of plaque forming units (PFU), which allowed the original phage stock to be adjusted to the desired concentration of $5 \times 10^7$ PFU/mL.

### 3.3. Preparation of scanning electron microscope (SEM) images

To assess deposition of bacteria on surfaces, 5 μL droplets of either *E. coli* (ATCC 13706) or *P. syringae* (ATCC 21781) were placed on a test section and left to dry in an environment with RH = 60% and 22 °C. Once dried, the surfaces were immersed in a Petri dish containing 2.5% glutaraldehyde for 18 h, then washed with sterile phosphate buffered saline (PBS, 0.85 wt% NaCl), placed in increasing concentrations (20%, 40%, 60%, 80%) of ethanol for 30 min each, and then submerged in 100% ethanol for 30 min, twice. The surfaces were then left to dry in a

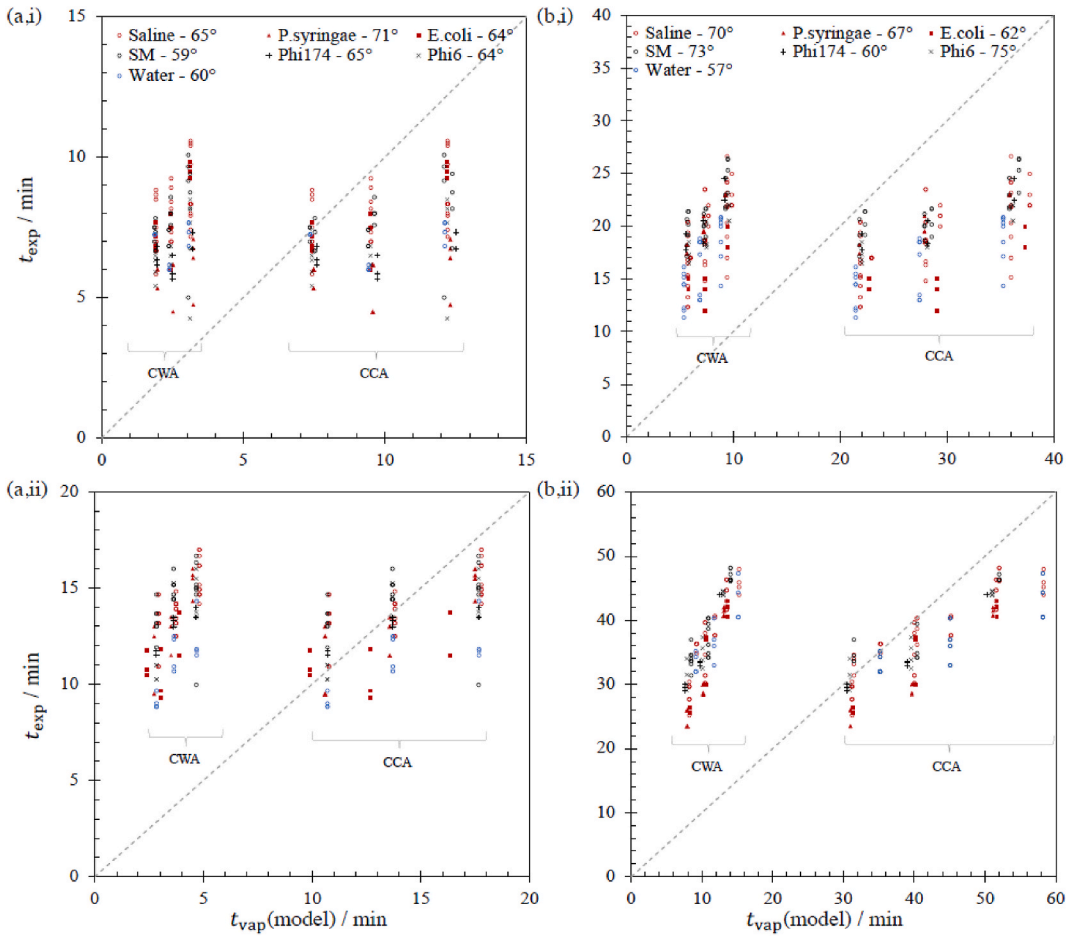


**Fig. 9.** Comparison of liquid drop evaporation times in stagnant air on PVC with CCA and CWA model predictions. Liquid drops with initial volume of (i) 1 μL or (ii) 5 μL, and at (*a*) low humidity and (*b*) mid humidity at temperatures of 22, 26 and 30 °C. Dashed locus shows the line of equality, *i.e.* $y = x$. *P. syringae* and *E. coli* prepared in saline, *Phi X174* and *Phi6* in SM buffer. The contact angle indicated in the legend is the measured static contact angle of the liquid drop on the PVC surface (see Tables 2 and 3).

vacuum sealed desiccator for a minimum of 18 h. Samples were then mounted onto aluminium pin stubs using adhesive carbon tabs and coated with a thin layer (25 nm) of Au metal using a sputter coater (Polaron, 30 s, 800 V, 5 mA). The stubs were then loaded into the FE-SEM (Carl Zeiss Ltd, Supra 40VP, SmartSEM) for imaging and analysis. The secondary electron detector was used to obtain images of the samples, using an acceleration voltage of 2 kV and a working distance of approximately 5 mm.

### 3.4. Measurement of contact angles

Images of droplets on each material were captured by pipetting droplets of 1 μl or 5 μl on to the surface, followed by measuring the contact angle (average of left and right tangent contact angles) using a goniometer (Krüss mobile drop GH11). Droplets were assessed in triplicate and each measurement was performed on a different coupon of material. To ascertain if contact angles for each liquid type on each material can be considered the same or statistically significantly different ($p < 0.05$), a *t*-test was performed comparing contact angles at 1 μl and 5 μl.

### 3.5. Evaporation of solutions and suspensions

To assess the impact of the presence of microorganisms on the time it takes droplets to dry, droplets of saline containing either *E. coli* (ATCC 13706) or *P. syringae* (ATCC 21781) were compared with droplets of saline without bacteria. Additionally, droplets of SM buffer containing either Phi6 (ATCC 21781-B1) or PhiX174 (ATCC 13706-B1) bacteriophage were compared with droplets of SM buffer without bacteriophage. Droplets of either 1 ± 0.1 μL or 5 ± 0.2 μL volume were deposited on a test section by pipette. The time taken for each droplet to dry as observed visually was recorded. To ensure measurement of drying time was consistent, data were collected by one researcher who used a digital stopwatch to record the time each droplet took to evaporate. Droplets were observed by eye continuously and the time by which the droplet had evaporated was taken as when no moisture was apparent.

## 4. Results and discussion

### 4.1. Evaporation of water droplets

Redfern et al. studied the effect of temperature and humidity on the evaporation of water droplets from a polypropylene surface. The range of conditions investigated is summarised in Table 1, along with the range of associated characteristic evaporation times $t_c$ (see Equation [5]). The humid air (an air-water mixture) was treated as an ideal gas with thermophysical properties taken from standard texts. The mol fraction of water vapour in equilibrium with the liquid over the temperature range of interest followed $y^* = 0.000054T^2 - 0.031T + 4.31$, where $T$ is in Kelvin. The contact angle for static droplets was reported as 83.4°, which is smaller than those reported in the literature (96.7° - Rios et al., 2007; 104.9° - Choi et al., 2019). The (advancing) contact angle

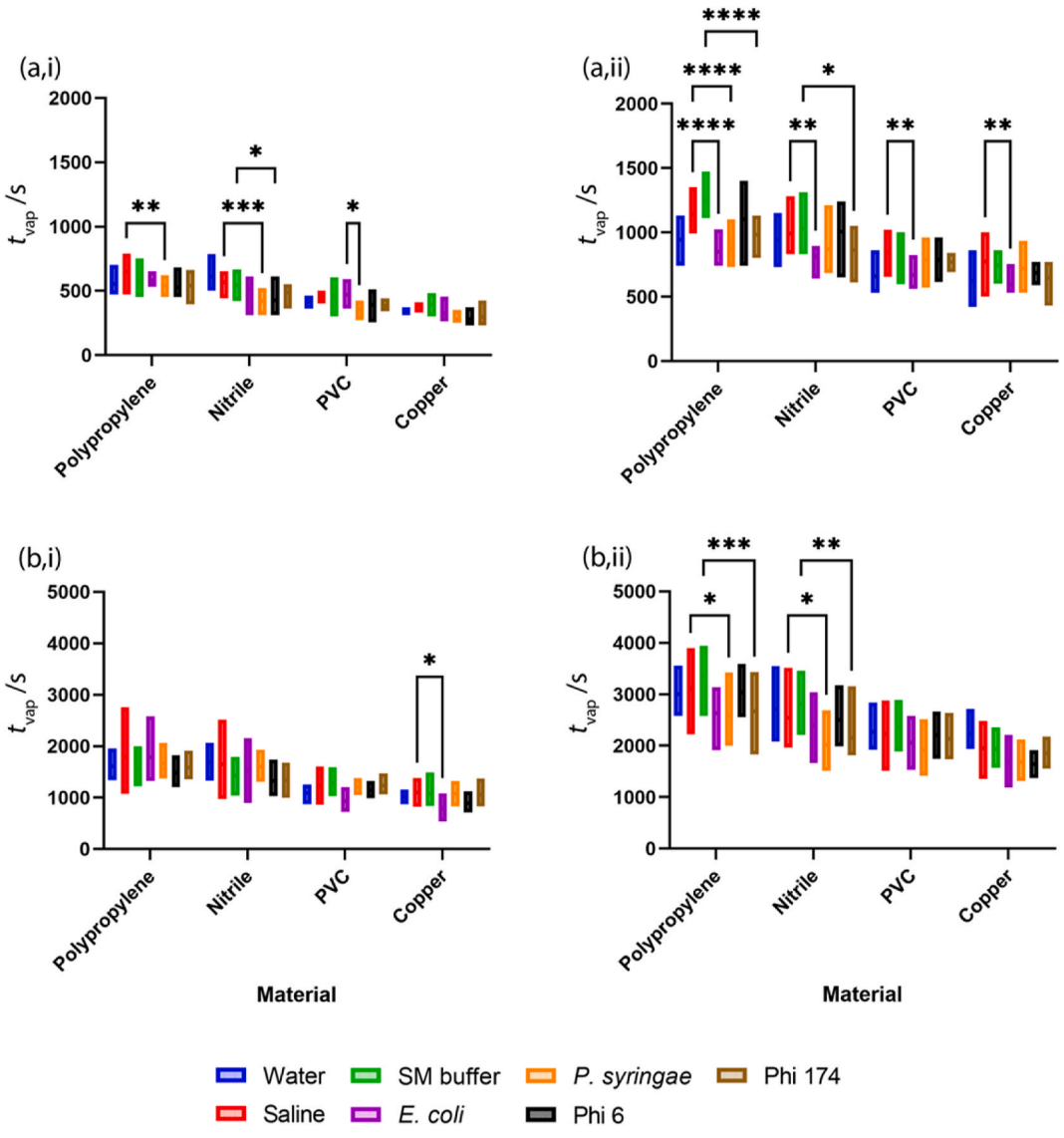


**Fig. 10.** Effect of material on droplet drying times. (a,i) 1 μL droplets in low RH, (a,ii) 1 μL droplets in medium RH, (b,i) 5 μL droplets in low humidity and (b,ii) 5 μL droplets in medium humidity. All measurements were at room temperature (18 °C). Statistical significance is shown for comparisons of bacteria vs. saline and bacteriophage vs. SM buffer and are represented as follows: * - $p \leq 0.05$, ** - $p \leq 0.01$, *** - $p \leq 0.001$ and **** - $p \leq 0.0001$.

for water measured on polypropylene for the experiments conducted in this work, 103° (Table 4), is consistent with the literature values.

Three convection conditions were considered:

(a) Quasi-stagnant conditions, where there was no forced convection so mass transfer was determined by diffusion: estimates of natural convection indicated that this had little effect in this case;
(b) Fan, half power.
(c) Fan, full power.

The local bulk air velocity in the vicinity of the droplet in (*b*) and (*c*) was estimated using a computational fluid dynamics package (see Redfern et al.): these varied from 0.5 m $s^{-1}$ to 1.9 m $s^{-1}$, corresponding to droplet Reynolds number, $Re_d = \frac{UR_0}{\nu}$, values of 140–550.

#### 4.1.1. Stagnant air

Fig. 4 compares the observed evaporation times for each droplet volume with the values predicted for water by the two contact modes (CCA, CWA). The evaporation time increases with droplet volume, as expected (since $t_c \propto R_0^2 \sim V_d^{2/3}$). The data points lie close to the CCA prediction, shown by the line of equality, whereas the CWA mode predicts consistently shorter evaporation times. Given the variation in temperatures, humidity and droplet volume, this level of agreement is considered good.

Also shown on the figure are the predictions of the mixed model, where the initial stage of evaporation follows CWA behaviour until the receding contact angle, $\theta_r$, is reached. The latter parameter was set at $\theta_r = \theta_a/1.2$ as this gave reasonably good agreement. This is an interesting result which does not appear to be considered in studies on droplet evaporation, even though it could be expected: a droplet striking a surface would be expected to spread on contact, when it is subject to the advancing contact angle, but on evaporation it will switch to receding angle behaviour.

#### 4.1.2. Forced convection

Activating the fan increased the rate of evaporation, but not in a systematic manner, unlike studies of droplet mass transfer in well-defined duct flows (*e.g.* Coutant and Penski, 1982; Ganzevles and van der Geld, 1998). Fig. 5 shows the effect of convection, expressed as $Re_d$, on observed evaporation times. The fan speeds were not sufficiently

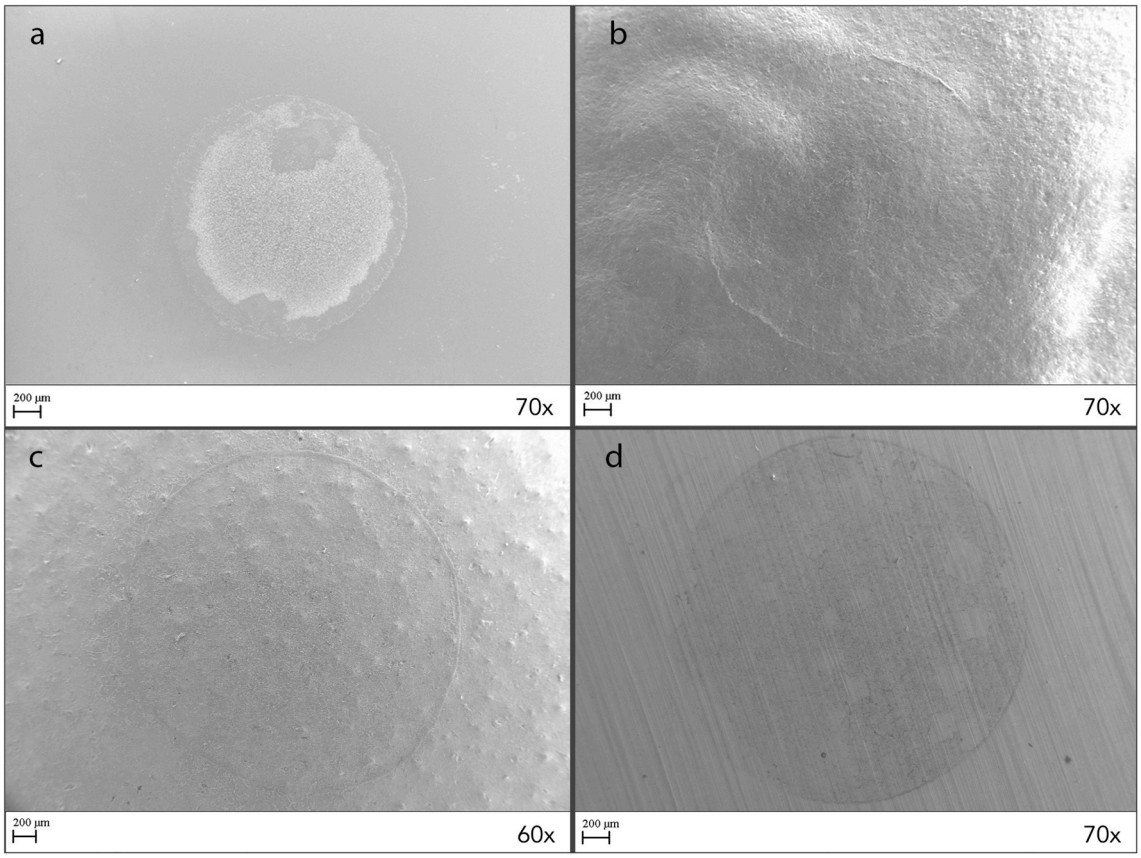


**Fig. 11.** SEM images of (A) polypropylene, (B) nitrile, (C) PVC and (D) copper surfaces following evaporation of a 5 μl droplet containing *E. coli* at RH = 60% and 22 °C.

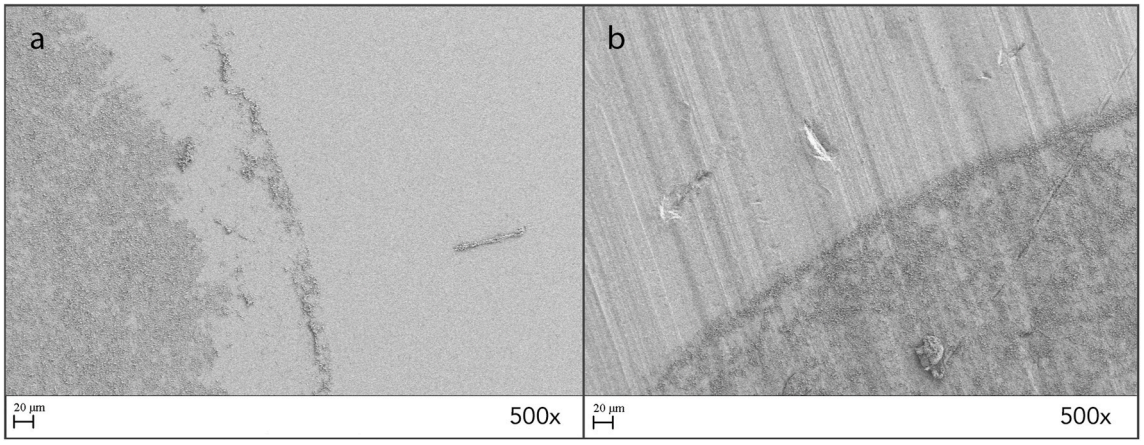


**Fig. 12.** Higher resolution SEM images of (a) polypropylene and (b) copper surfaces (see Fig. 11(a),(d)) following evaporation of a 5 μl droplet containing *E. coli* at RH = 60% and 22 °C.

large to cause the droplets to move across the surface. The times are divided by the value predicted for CCA (Fig. 5(a)) and CWA (Fig. 5(b)) behaviour. Effects such as shear-induced change in droplet shape were not considered. The values for quasi-stagnant air are plotted for comparison: for these $Re_d$ was calculated with a velocity of 1 mm $s^{-1}$. There is a general decrease in evaporation time with $Re_d$, with noticeable scatter as other test conditions are manipulated. The effect of convection is also expected to depend on the Schmidt number, $Sc \equiv \frac{\mu}{\rho D}$ (where $\rho$ is the mass density, see Coutant and Penski, and Ganzelves and van der Geld): this parameter did not vary strongly over the conditions considered here. Fig. 5(a) shows that the experimental values obtained under quiescent conditions lie consistently closer to the CCA predictions.

The effect of draughty conditions can be estimated for these droplets by exploiting the fact that the contact angle is close to 90°, so that they can be approximated as hemispheres. The Sherwood number can then be estimated from the Ranz and Marshall correlation (1952) for mass transport from spheres, *viz.*

$$\overline{Sh} = 2 + 0.6 Re^{1/2} Sc^{1/3} \quad [10]$$

which, for the Reynolds and Schmidt numbers considered here, would give values of $\overline{Sh}$ ranging from (initially) 6.1 to 14.2, decreasing to 2 as

the droplet evaporated. Taking a geometric mean of these values as a rough estimate of the Sherwood number over a droplet's evaporation time would give $t_{exp}/t_{vap}$(CWA) ~ 0.37–0.56 for the cases with forced convection, which is consistent with the observed range of values. The need to consider convection when conducting tests and applying the results to practice is evident.

### 4.2. Evaporation of solutions and suspensions

The rate of evaporation of droplets containing organisms was studied using 1 μL and 5 μL droplets on four surfaces under conditions of mild (40–47% RH) and low humidity (14–16% RH). Macroscopic advancing contact angles on each surface were determined for 1 μL and 5 μL droplets of water, saline and SM buffer as well as the suspensions. The goniometer system used was not a precision device and the results, summarised in Tables 2 and 3, are used to identify trends. Most of the $\theta_a$ values lie in the range 45–90°. With 1 μL droplets (Table 2), the presence of *E. coli* gave different contact angles to the neat saline on nitrile and copper; by comparison, *P. syringae* gave values closer to the saline. The Phi6 and PhiX174 suspensions gave similar (within ~10°) values on nitrile, PVC and copper: on nitrile, these were different to the neat SM buffer. With the 5 μL drops (Table 3), the contact angles for neat saline, SM buffer and water were similar for all materials except copper, where SM buffer was lower. The contact angles for *E. coli* and *P. syringae* on polypropylene and copper were similar to those with saline, while those on nitrile were noticeably lower. The contact angles for SM buffer and Phi6 and PhiX174 suspensions were similar with the exception of copper and PVC, where PhiX174 was higher and lower respectively.

#### 4.2.1. Evaporation times

The salts present in the saline solution (0.85 wt% NaCl) and SM buffer (see method section for composition) reduce the vapour pressure exerted by the water and the initial driving force for mass transfer, $\Delta y$, but this proved to be a small effect for the low and mid-humidity cases considered here. For the saline solution, the initial reduction in $\Delta y$ is of the order of 0.26% at room temperature. If the solutes remain in solution and are not adsorbed on to the surface, one could then expect either (i) evaporation to stop as $\Delta y$ approached zero, or (ii) the salts to undergo crystallisation, producing precipitates which would be visible under the microscope. Crystals were not evident in SEM images of the dried surfaces (with the exception of *P. syringae* on nitrile, see Supplementary Figure S1) and experiments with neat saline and buffer solutions all evaporated completely, indicating that salts were adsorbed on to the wetted surface.

Fig. 6 shows the effect of droplet composition on drying times, presented in the same format as the Redfern et al. results for water droplets in Fig. 4. A different polypropylene surface was used in these experiments. The observed evaporation times are in broad agreement with the CCA model predictions, as seen in Fig. 4. At low humidity (Fig. 6(a) - faster evaporation rates), the use of saline tends to increase the evaporation times compared to water, whereas the SM buffer times are similar to those for water. This effect is more noticeable with the mid-humidity data (Fig. 6(b)), in which case both saline and SM buffer exhibit longer evaporation times than water. This trend is noted in Table 4, alongside the trends observed for the other surfaces (Figs. 7–9).

The presence of organisms tends to reduce the evaporation time for both saline and SM buffer droplets. This suggests that the species are promoting CWA behaviour, which would be consistent with organisms collecting at the evaporation front, promoting pinning behaviour (but not necessarily fixing the contact line). The trends are recorded in Table 4 and are compared with the observed deposition patterns in the next section. Evaporation times were faster in the low humidity scenarios for both 1 μl and 5 μl droplet sizes, which is consistent with Equations [5] and [8], where $t_c \propto \Delta y^{-1}$.

Further analysis comparing evaporation times of droplets containing microorganisms with either saline or SM buffer alone revealed that in all cases of statistically significant differences ($p < 0.05$, $n = 11/32$ for bacteria and $n = 6/32$ for bacteriophages), the addition of microorganisms resulted in more rapid evaporation (Fig. 10). When comparing the total number of significantly different evaporation times with respect to RH, medium RH (40%) conditions provided a larger number of droplets that evaporated more quickly due to the presence of a microorganism, in both 1 μL and 5 μL scenarios. When comparing evaporation times with respect to droplet size, 1 μL droplets containing microorganisms evaporated significantly more rapidly than ones without more often (than 5 μL droplets) in both low (15%) and medium (40%) RH scenarios.

#### 4.2.2. SEM images of bacterial deposition

The deposition patterns created by evaporation of 5 μL droplets containing *E. coli* or *P. syringae* differed depending on the substrate material. Whilst a ring marking the initial boundary of the droplet (*i.e.* the initial contact line) was visible on all images (see *E. coli* examples in Fig. 11), deposition of bacteria within the droplet footprint was more evident on polypropylene and copper (Fig. 12) unlike on nitrile and PVC where deposition within the footprint was less obvious (Figure S2). On polypropylene the bacteria were deposited with an obvious outer ring, *i.e.* bacteria deposited in a circular ring at the outer edge followed by an annulus where no bacteria were deposited, followed by an inner region where the majority of bacteria were deposited. In contrast, no annular region is apparent in the copper case. Deegan et al. (2000) discussed how differences in evaporation flux and change of height profile can promote coffee ring or uniform deposition behaviour: further work would be required to see if this is the reason for these observations.

Comparing the evaporation time plots (Fig. 6(b,ii) – polypropylene and Fig. 8(b,ii) – Cu), on copper the values consistently lay below the CCA line, suggesting mixed mode drying, while on polypropylene the data showed a strong correlation with CCA behaviour. Further work is needed to link deposition behaviour and drying kinetics: Deleplace et al. (2022) reported very pronounced deposition of *Bacillus* spores at the initial contact line on the four surfaces they studied, followed by different patterns in the footprint depending on the surface nature-species combination. In both instances in Fig. 12, bacteria are highly concentrated in different areas, resulting in deposition of bacterial cells on top of one another.

## 5. Discussion

A combination of modelling and experimental methods have been used to investigate the impact of microorganisms on the evaporation of liquid droplets on solid surfaces. The four surfaces studied are representative of many materials that are found in hospitality, healthcare and food processing facilities. They were not strongly wetting towards water (contact angles ranging from approximately 40°–100°), so that droplets formed or landing on the surface would tend to remain spherical rather than spread out to form a thin film.

The first order (external mass transfer control) model for the time taken for a droplet to evaporate provides useful insights into how the drying dynamics are determined by the contact angle and whether the droplet exhibits contact line pinning, which would be expected to promote constant wetted area behaviour. The evaporation times observed with water alone (Fig. 4) show good agreement with the values predicted for constant contact angle behaviour, and better agreement with the mixed model which incorporates a reasonable switch between the advancing contact angle, associated with the initial contact of the droplet on the surface, and the receding value. The predictions for constant wetted area behaviour, which might be associated with contact line pinning, give consistently poor agreement with the experimental measurements.

The addition of bacteria reduced the evaporation time significantly for all surface types in at least one of each droplet size/RH scenarios, whereas the addition of bacteriophage did not decrease the evaporation

time significantly on PVC or copper in any droplet size/RH scenario. Overall, the 1 μL droplets tend to exhibit less variation in drying time and dried more quickly than the 5 μL droplets, as expected from the model. The models did not capture the effect of adding bacteria or bacteriophage on the drying times, but the experimental values were, nevertheless, consistently closer to the constant contact angle scenario predictions rather than the constant wetted area ones, indicating that the deposition of these microorganisms does not give rise to the contact line pinning effects reported with colloidal suspensions. The bacteria, with sizes greater than 1 μm, are not expected to give rise to colloidal behaviour, whereas the bacteriophage, with lengths 20–30 nm, might if they did not agglomerate when suspended. Electron microscopy of images of the phages on the surface indicated that agglomerate and network formation did occur, but it was not possible to determine if this happened before they deposited on the surface.

Figs. 6–9 indicate that further work is required to capture the impact of these species on the drying kinetics, given that the constant contact angle model gives a reasonable working estimate of the evaporation time. Considering the input parameters to the model, the factor subject to most uncertainty is the effective contact angle. The values used in the calculations were taken from static observations of the solutions or suspensions on dry solid surfaces, whereas the images of the droplet footprints after drying indicated that these were no longer even and uniform, but rough and heterogeneous as a result of organism deposition. For wetting liquids, the Wenzel model predicts that a rougher surface will result in a smaller effective contact angle (the surface becomes more wetting) and Fig. 3 shows that reducing $\theta$ will reduce $F_\theta$ and the evaporation time. This enhanced roughness hypothesis could explain the observed reduction in evaporation times for the suspensions: predicting the magnitude of the effect would require knowledge of the deposition pattern and structure and is beyond the scope of the current work.

Given that moisture is required for many antimicrobial materials to exhibit antimicrobial activity, understanding that the presence of microorganisms can increase the rate at with evaporation occurs is important, as a shorter evaporation time will also result in reduced antimicrobial activity. Therefore, for those interested in the development, manufacture and installation of antimicrobial materials, it is essential to consider what type of microbial contamination the user is trying to control and use this knowledge in the development of their initial antimicrobial efficacy assessment methods.

## 6. Conclusions

This cross-disciplinary study revealed that the application of quantitative models for the kinetics of moisture evaporation on surfaces can help to explain and interpret findings when testing for the efficacy of antimicrobial surfaces. The speed of droplet evaporation is affected by a range of factors: temperature, humidity, airflow, the nature of the surface and the presence (and nature) of microorganisms. The kinetics of droplet evaporation affects the presence of moisture on a surface, and thence the survival of microorganisms and, potentially, the mode of action of putative antimicrobial agents in/on the surface – particularly if the agents require moisture for activity. Standardised testing methods provide detailed accounts of procedures, but do not always specify with any precision, the ambient conditions where testing takes place. If these factors are not adequately recognised or controlled, results from testing methods performed under different (or unspecified) environmental conditions in different laboratories are liable to vary and give rise to confusion, misinterpretation, and potentially misleading claims of effectiveness.

## Credit author statement

Alexander J. Cunliffe: Investigation, Methodology, Validation, Visualization, Conceptualization, Data curation, Formal analysis, Writing – original draft, Writing – review & editing, Ru Wang: Investigation, Methodology, Validation, Visualization, Conceptualization, Data curation, Formal analysis, Writing – original draft, Writing – review & editing, James Redfern: Methodology, Visualization, Project administration, Resources, Supervision, Conceptualization, Formal analysis, Writing – original draft, Writing – review & editing, Joanna Verran: Methodology, Supervision, Resources, Conceptualization, Writing – review & editing, Ian Wilson: Methodology, Visualization, Supervision, Conceptualization, Formal analysis, Writing – original draft, Writing – review & editing.

## Data – open access

All data created during this research is openly available from Manchester Metropolitan University's research repository: https://doi.org/10.23634/MMU.00629876.

## Declaration of competing interest

The authors declare that they have no known competing financial interests or personal relationships that could have appeared to influence the work reported in this paper.

## Acknowledgements

A PhD studentship for RW from the WD Armstrong Fund is gratefully acknowledged. Match-funding for a PhD studentship for AJC from the International Biodeterioration Research Group is gratefully acknowledged.

## Appendix A. Supplementary data

Supplementary data to this article can be found online at https://doi.org/10.1016/j.jfoodeng.2022.111195.

## Appendix

Fig. 2 shows that it takes approximately 4 min for the salt solutions to re-establish the desired relative humidity within the chamber after the lid was replaced. The dynamics are consistent with mass transfer control: let the rate of evaporation from the surface of the salt solution can be expressed as a molar flux, $N$, where

$$N = \overline{k_m} C_T (y^* - y_b) \quad [A1]$$

where $\overline{k_m}$ is a mass transfer coefficient, $y_b$ is the mol fraction of water in the air, and $C_T$ the molar density of the air (given by $P/R_G T$, where $P$ is the total pressure, $R_G$ the gas constant and $T$ the absolute temperature). At the surface of the salt solution the water in the vapour will be in equilibrium with that in the salt solution, with mol fraction $y^*$. For the closed system when the lid is closed, a mass balance gives

$$\frac{d}{dt}(VC_T y_b) = A_s \overline{k_m} C_T (y^* - y_b) \quad [A2]$$

where $V$ is the volume of the vapour in the chamber, $t$ is time, and $A_s$ is the area of solution surface available for mass transfer. This assumes perfect mixing in the vapour phase. Assuming isothermal operation so that the parameters are constant gives

$$ln\left\{\frac{(y^* - y_{b,o})}{(y^* - y_b)}\right\} = ln\left\{\frac{(RH^* - RH(0))}{(RH^* - RH(t))}\right\} = \frac{A_s \overline{k_m}}{V} t \quad [A3]$$

with $y_{b,o}$ the mol fraction of water in the air at the start of the experiment. For dilute concentrations, $RH \propto y$ (McCabe et al., 1993) and Equation [A3] indicates that a plot of $-ln(RH^* - RH(t))$ against $t$ should be linear with gradient proportional to the ratio of the surface area of the salt reservoirs to the volume of the chamber.

## References


Adams, M.H., 1959. *Bacteriophages*, Publ. Interscience Publishers.

BS ISO 22196, 2011. 2011 Measurement of Antibacterial Activity on Plastics and Other Non-porous Surfaces. BSI, London.

Bormashenko, E.Y., 2017. Physics of Wetting. publ. De Gruyter.

Chatterjee, S., Murallidharan, J.S., Agrawal, A., Bhardwaj, R., 2021. Why coronavirus survives longer on impermeable than porous surfaces. Phys. Fluids 33, 021701.

Choi, H.-J., Kim, M.S., Anh, D., Yeo, S.Y., Lee, S., 2019. Electrical percolation threshold of carbon black in a polymer matrix and its application to antistatic fibre. Sci. Rep. 9 (1), 6338.

Coutant, R.W., Penski, E.C., 1982. Experimental evaluation of mass transfer from sessile drops. Ind. Eng. Chem. Fund. 21, 250–254.

Cunliffe, A.J., Askew, P.D., Stephan, I., Iredale, G., Cosemans, P., Simmons, L.M., Verran, J., Redfern, J., 2021. How do we determine the efficacy of an antibacterial surface? A review of standardised antibacterial material testing methods. *Antibiotics* 10, 1069. https://doi.org/10.3390/antibiotics10091069.

Deegan, R.D., Bakajin, O., Dupont, T.F., Huber, G., Nagel, S.R., Witten, T.A., 1997. Capillary flow as the cause of ring stains from dried liquid drops. Nature 389, 827–829.

Deegan, R.D., Bakajin, O., Dupont, T.F., Huber, G., Nagel, S.R., Witten, T.A., 2000. Contact line deposits in an evaporating drop. Phys. Rev. 62, 756–765.

Deleplace, M., Dallagi, H., Dubois, H., Richard, E., Ipatova, A., Benezech, T., Faille, C., 2022. Structure of deposits formed by drying of droplets contaminated with *Bacillus* spores determines their resistance to rinsing and cleaning. J. Food Eng. 318, 110873.

Eales, A.D., Dartnell, N., Goddard, S., Routh, A.F., 2016. Thin, binary liquid droplets, containing polymer: an investigation of the parameters controlling film shape. J. Fluid Mech. 794, 200–232.

Ganzevles, F.L.A., van der Geld, C.W.M., 1998. Heat and mass transfer from internal flows to hemispheres and flat parts in between. Int. J. Heat Mass Tran. 41, 3705–3718.

Grass, G., Rensing, C., Soliozm, M., 2011. Metallic copper as an antimicrobial surface. Appl. Environ. Microbiol. 77 (5), 1541–1547.

Hansan, Abshar, Lee, Kyueui, Tewari, Kunal, Pandey, Lalit M, Messersmith, Phillip B, Faulds, Karen, Maclean, Michelle, Lau, King Hang Aaron, 2020. Surface Design for Immobilization of an Antimicrobial Peptide Mimic for Efficient Anti-Biofouling. Chemistry 7 (26), 5789–5793. https://doi.org/10.1002/chem.202000746.

Hu, H., Larson, R.G., 2002. Evaporation of a sessile droplet on a substrate. J. Phys. Chem. B 106, 1334–1344.

Imani, S.M., Ladouceur, L., Marshall, T., Maclachlan, R., Soleymani, L., Didar, T.F., 2020. Biomaterials-based formulations and surfaces to combat viral infectious diseases. APL Bioeng. 14, 12341–12369.

Kumari, S., Chatterjee, K., 2021. Biomaterials-based formulations and surfaces to combat viral infectious diseases. APL Bioeng. 5, 011503.

Larson, R.G., 2014. Transport and deposition patterns in drying sessile droplets. AIChE J. 60 (5), 1538–1571.

McCabe, W.L., Smith, J.C., Harriott, P., 1993. Unit Operations of Chemical Engineering. McGraw-Hill, NY. Ch. 23, publ.

Rai, M., Yadav, A., Gade, A., 2009. Silver nanoparticles as a new generation of antimicrobials. Biotechnol. Adv. 27 (1), 76–83.

Ranz, W., Marshall, W., 1952. Evaporation from drops. Chem. Eng. Prog. 48, 141–146.

Ratova, M., Redfern, J., Verran, J., Kelly, P.J., 2018. Highly efficient photocatalytic bismuth oxide coatings and their antimicrobial properties under visible light irradiation. Appl. Catal. B Environ. 239, 223–232.

Rios, P.F., Dodiuk, H., Kenig, S., McCarthy, S., Dotan, A., 2007. The effect of polymer surface on the wetting and adhesion of liquid systems. J. Adhes. Sci. Technol. 21 (3–4), 227–241.

Redfern, J., Tucker, J., Simmons, L.M., Askew, P., Stephan, I., Verran, J., 2018. Environmental and experimental factors affecting efficacy testing of non-porous plastic antimicrobial surfaces. Methods Protocols 1, 36. https://doi.org/10.3390/mps1040036.

Sobac, B., Brutin D, D., 2011. Triple-line behavior and wettability controlled by nanocoated substrates: influence on sessile drop evaporation. Langmuir 27, 14999–15007.

Soulié, V., Karpitschka, S., Lequien, F., Prené, P., Zemb, T., Moehwald, H., Riegler, H., 2015. The evaporation behavior of sessile droplets from aqueous saline solutions. Phys. Chem. Chem. Phys. 17, 22296–22303.


## Nomenclature

### Roman symbols

$A_d$: Area of liquid-air interface $m^2$
$A_S$: Area of solution-air interface $m^2$
*Bo:* Bond number
$C_T$: Total molar concentration, vapour phase mol $m^{-3}$
$D$: Diffusivity $m^2\ s^{-1}$
$F_L$: Factor, constant wetted area
$F_\theta$: Factor, constant contact angle
$g$: Gravitational acceleration m $s^{-2}$
*H:* Humidity ?
$\overline{k_m}$: Average mass transfer coefficient m $s^{-1}$
*L:* Radius of wetted area m
*n:* Number of samples
*N:* Molar flux mol $m^2 s^{-1}$
*p: p*-value from a statistical test Pa
*P:* Total pressure Pa
$Re_d$: Droplet Reynolds number
*R:* sphere radius m
$R_G$: Gas constant J $mol^{-1} K^{-1}$
$R_0$: Initial droplet radius m
$R^2$: Correlation coefficient
*Sc:* Schmidt number
$\overline{Sh}$: Mean Sherwood number
*t:* Time s
$t_c$: Characteristic time s
$t_{exp}$: Droplet evaporation time (experimental values) s
$t_{vap}$: Droplet evaporation time (calculated from models) s
*T:* Temperature K
*V:* Volume of vapour $m^3$
$V_d$: Volume of drop $m^3$
$y$, $y_b$, $y^*$: Mol fraction in vapour phase, bulk phase value, saturated value

### Greek symbols

$\gamma$: Vapour-liquid surface tension N $m^{-1}$
$\mu$: Liquid dynamic viscosity Pa s
$\nu$: Kinematic viscosity $m^2\ s^{-1}$
$\Delta\rho$: Difference in mass densities kg $m^{-3}$
$\rho_m$: Liquid molar density mol $m^{-3}$
$\theta$: Contact angle °
$\theta_a$, $\theta_a$: Advancing, receding contact angle °

### Acronyms

*CCA:* Constant contact angle
*CWA:* Constant wetted area
*PFU:* Plaque forming units
*PVC:* Polyvinylchloride
*RH:* Relative humidity
*SMB:* SM Buffer
*SEM:* Scanning electron microscopy
*TSA:* Tryptone soya agar